


Optimal Multivariable MMC Energy-Based Control for DC Voltage Regulation in HVDC Applications

Journal Article**Author(s):**

Sanchez-Sanchez, Enric; [Gross, Dominic](#) ; Prieto-Araujo, Eduardo; [Dörfler, Florian](#) ; Gomis-Bellmunt, Oriol

Publication date:

2020-04

Permanent link:

<https://doi.org/10.3929/ethz-b-000357748>

Rights / license:

[In Copyright - Non-Commercial Use Permitted](#)

Originally published in:

IEEE Transactions on Power Delivery 35(2), <https://doi.org/10.1109/tpwrd.2019.2933771>

Funding acknowledgement:

691800 - Massive InteGRATion of power Electronic devices (SBFI)

Optimal Multivariable MMC Energy-Based Control for DC Voltage Regulation in HVDC Applications

Enric Sánchez-Sánchez, *Student Member, IEEE*, Dominic Groß, *Member, IEEE*,
Eduardo Prieto-Araujo, *Member, IEEE*, Florian Dörfler, *Senior Member, IEEE*,
and Oriol Gomis-Bellmunt, *Senior Member, IEEE*

Abstract—The penetration of renewable energy resources is changing the way the power system is understood and operated. With an increasing number of power electronics devices integrated into the power system, the MMC is arising as one of the key technologies for HVDC applications. While several control strategies for MMCs have been proposed in the last years, designing controls for MMCs remains a challenging and non-trivial problem due to its large number of degrees of freedom. In this paper, a general multivariable control structure is proposed that generalizes and improves upon previously reported approaches. Moreover, to fully exploit the degrees of freedom offered by this control, a model-based tuning methodology is presented that extends results from optimal \mathcal{H}_2 structured control design to MMC applications. A case study using an HVDC link is used to illustrate and analyze the performance of the MMC using the proposed approach in different scenarios.

Index Terms—HVDC, MMC, control, optimal tuning.

I. INTRODUCTION

IN modern power systems, the penetration of power electronics devices is rising, mainly due to the increase of renewable energy integration. One of the main applications of power electronics in today's power system are High Voltage Direct Current (HVDC) links, used in applications such as offshore wind farms and very long overhead lines [1]. The Modular Multilevel Converter (MMC) has emerged as the preferred converter topology for HVDC due to its efficiency, scalability, and inherent redundancy [2], [3]. Compared to the classic two-level (2L) voltage source converter (VSC), control of MMCs is more challenging because the MMC topology offers more degrees of freedom and the complex dynamics of MMC systems typically span multiple time scales.

Based on how the modulation indexes are calculated, two different control approaches can be found in the literature. In the non-energy-based approach, also known as uncompensated

modulation (UCM) or direct voltage control, the energy is not explicitly controlled [4]–[8]. While such an approach renders the overall system asymptotically stable, parasitic circulating current components appear, and they are usually suppressed with additional current control loops [4]. Even so, the resulting dynamics and control performance depend on the converter impedance, and this usually leads to slow convergence and undesired overshoots, especially during faults [9]. In contrast, in the energy-based approach, also known as compensated modulation (CM) or closed-loop modulation, the calculation of the modulation indexes compensates for the oscillations in the arm capacitors voltages [9]–[12]. This approach does not rely on parasitic components, but additional energy control loops are required to obtain an asymptotically stable and balanced system [13]. Overall, the energy-based approach leads to an improved transient performance [9] and an improved stability [14].

Focusing on the energy-based approach applied to a converter that controls the DC voltage (master converter), the classic structure for the outer control consists of a DC voltage controller that generates the AC grid current reference, and an energy controller that generates the zero-sequence (DC) circulating current reference [9], [10], [15]. However, because the MMC does not include a large DC capacitor its DC effective capacitance depends on external elements such as cables. For relatively short cables, this effective capacitance is small. In those cases, the classic control structure does not perform well, and the voltage control needs to be further addressed. Even though HVDC links of few tens of kilometers are not frequent, some applications are already in operation. Moreover, cables of only few kilometers might be used in future applications, such as interconnecting neighboring systems with different frequencies or phase angles (non-synchronous). To mitigate issues arising from short cable lengths, the classic control structure has been extended with an additional virtual capacitor control that uses the internal energy of the MMC to reinforce the equivalent DC capacitance of the system [16]. This is done by means of calculating the energy reference as a function of the DC voltage measurement, thereby providing an extra degree of freedom.

Compared to the standard classic structure, the performance can be improved with a cross structure, which connects the outer controllers to the opposite inner controllers (i.e., opposing the standard interconnection), thereby resulting in a better decoupling between the AC and DC sides [17], [18]. Furthermore, a weighted structure connecting both PI outputs

This work was partially funded by FEDER / Ministerio de Ciencia, Innovación y Universidades - Agencia Estatal de Investigación, Project RTI2018-095429-B-I00, by the FI-AGAUR Research Fellowship Program, Generalitat de Catalunya, by the InnoEnergy PhD School Programme, European Institute of Technology (EIT), and by the European Union's Horizon 2020 research and innovation programme under grant agreement N° 691800. This article reflects only the authors' views and the European Commission is not responsible for any use that may be made of the information it contains.

E. Sánchez-Sánchez, E. Prieto-Araujo, and O. Gomis-Bellmunt are with the Centre d'Innovació Tecnològica en Convertidors Estàtics i Accionaments, Departament d'Enginyeria Elèctrica, Universitat Politècnica de Catalunya, Barcelona 08028, Spain. E. Prieto-Araujo is also a Serra Hünter Lecturer (e-mail: enric.sanchez.sanchez@citcea.upc.edu; eduardo.prieto-araujo@citcea.upc.edu; oriol.gomis@upc.edu)

D. Groß and F. Dörfler are with the Automatic Control Laboratory, ETH Zürich, Switzerland. (e-mail: gross@control.ee.ethz.ch; dorfler@ethz.ch)

to both current references at the same time was presented in [18], combining the effect of the classic and the cross structures. However, no insights were given with respect to the selection of the weights and tuning of the gains. The classic, cross and weighted control structures can be seen as special cases of a general multivariable control. However, no general and principled multivariable control design with an adequate (or even optimal) tuning method has been presented thus far.

The contribution of this paper is to introduce a multivariable control structure based on four independent PI controllers that generalizes and improves upon previously reported energy-based control structures. To fully exploit the degrees of freedom offered by this control and systematically treat the complex dynamics of MMC-based HVDC systems, results from \mathcal{H}_2 optimal structured control design are extended to obtain a systematic optimization-based tuning methodology. This method allows the formulation of the dynamic performance objectives in a systematic and intuitive way. Finally, we provide a case study that focuses on the critical case of short HVDC cables in which the voltage control needs to be tuned carefully and guidelines for manual tuning break down.

II. SYSTEM MODELING

A. Description of the system under study

The focus of the present study is the energy-based control approach for MMCs. More specifically, we consider an MMC that controls the voltage of the DC side (master converter), and synchronizes to the grid (*grid-following* converter) on the AC side (Fig. 1). A master converter typically operates in point-to-point HVDC links, which will be the case of the present study, and also in multi-terminal HVDC grids.

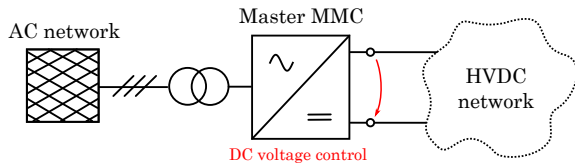


Fig. 1. Grid-connected MMC with DC voltage control.

One of the main challenges in the control of MMC-based point-to-point systems is controlling the DC voltage through the master converter when the DC equivalent capacitance is relatively small (i.e., for medium and short cables). In contrast, the slave converter with a standard control structure (i.e., an active power loop on top of the active current inner loop, and a total energy loop on top of a circulating current loop) performs adequately as long as the master converter is controlling the DC voltage properly. Therefore, we focus on improving the control of the master converter.

The MMC topology shown in Fig. 2 consists of six arms, each of them including N_{arm} half-bridge submodules with a capacitance C_{SM} , and an arm reactor in series. The submodules are controlled individually, either inserting or bypassing the capacitor. The three legs correspond to the three phases (a , b and c) each containing two arms. The six arms synthesize the required voltages in order to achieve the desired power exchange between the AC and the DC side and to handle the internal energy balance of the converter.

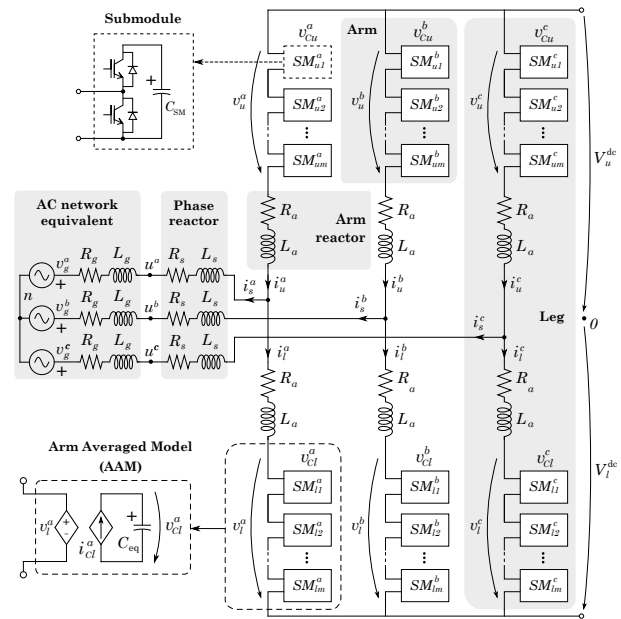


Fig. 2. Electrical model of the MMC connected to a grid Thévenin equivalent.

B. MMC model

As detailed in [9], [18], a coordinates transformation from *upper-lower* to *diff-sum* frame is useful to represent the system in state-space and to better identify the magnitudes to be controlled. The following variable change is defined

$$\begin{cases} v_{diff}^j \triangleq \frac{1}{2}(-v_u^j + v_l^j) \\ v_{sum}^j \triangleq v_u^j + v_l^j \\ i_{sum}^j \triangleq \frac{1}{2}(i_u^j + i_l^j) \end{cases}, \quad \begin{cases} R \triangleq R_s + R_g + \frac{R_a}{2} \\ L \triangleq L_s + L_g + \frac{L_a}{2} \end{cases}, \quad (1)$$

with

- v_{diff}^j : differential voltage (middle point of the arm),
- v_{sum}^j : additive voltage (approx. equal to the DC voltage),
- i_{sum}^j : additive current (from upper to lower arm),
- R_a, L_a : arm resistance and inductance,
- R_s, L_s : AC grid filter or transformer resistance and inductance,
- R_g, L_g : Thévenin AC grid resistance and inductance.

Assuming a balanced DC side, a balanced and grounded AC neutral point, and using the change of variables in (1) the AC side and circulating current equations are

$$v_{diff}^{abc} - v_g^{abc} = R\mathcal{I}_3 i_s^{abc} + L\mathcal{I}_3 \frac{di_s^{abc}}{dt} \quad (2)$$

$$v_{sum}^{abc} - V_t^{dc}(1 \ 1 \ 1)^T = -2R_a\mathcal{I}_3 i_{sum}^{abc} - 2L_a\mathcal{I}_3 \frac{di_{sum}^{abc}}{dt}, \quad (3)$$

where v_g^{abc} denotes the Thévenin AC grid voltage, i_s^{abc} is the AC grid current, i.e., $i_s^j = i_u^j - i_l^j$ for $j \in \{a, b, c\}$, and V_t^{dc} is the DC side voltage. Moreover, \mathcal{I}_n refers to a $n \times n$ identity matrix. The voltage applied by the arms and the current flowing through them may contain AC and DC components that affect the power exchange and energy stored in the converter

in different ways (see [9] for a detailed analysis). To complete the MMC model, an Average Arm Model (AAM) [19] is used for each arm (see Fig. 2). Each equivalent capacitor voltage v_{Cul}^{abc} depends on the power exchanged by each arm, which is reflected as a charging current i_{Cul}^{abc} in each capacitor circuit:

$$i_{Cul}^{abc} = C_{eq} \mathcal{I}_6 \frac{dv_{Cul}^{abc}}{dt} \quad (4)$$

C. Cable model

Selecting a suitable cable model is a crucial aspect in electromagnetic transient simulations. In this paper, we use the Universal Line Model (also known as wideband model) from the BestPaths open access Simulink toolbox [20] that captures the frequency dependent behaviour of the cable.

III. REVIEW OF CONTROL ARCHITECTURES

A. MMC energy-based control structures

In an energy-based control approach, the key aspect is that the total energy, the energy balance between arms (vertical balancing), and the energy balance between legs (horizontal balancing) has to be controlled. This is typically achieved using 6 PI controllers that may be combined with 3 additional PI controllers controlling the inner circulating current [9], [21] (see Fig. 3). The AC and DC sides control is equivalent to the 2L-VSC case, i.e., in the master MMC a DC voltage controller is required, whereas in the slave MMC an AC power controller is used instead. Once the six arms voltages references are computed, the submodules balancing algorithm and modulation strategy generate the corresponding switches signals [22].

Focusing on the master MMC, the outer DC voltage control, total energy controllers, and inner AC and DC circulating current controllers can be cascaded in different ways. The block diagram from Fig. 3 unifies the standard control structures. Depending on the choice of gains K_1 , K_2 , K_3 , and K_4 the classic, cross, and weighted structure are recovered:

- Classic control [9], [11], [15] without off-diagonal (cross) coupling, $K_2 = K_3 = 0$: this control structure is based on extrapolating the 2L-VSC structure to the MMC. The AC current reference (i_s^{q*}) is controlled by the DC voltage (V_t^{dc}) controller, whereas the DC circulating current reference (i_{sum}^{0dc*}) is controlled by the total energy (W_t) controller. When a DC voltage disturbance occurs, the first reaction will be through the AC current. This will affect the energy, which will be compensated through the DC current. A feed-forward of the AC power is usually added after the output of the total energy PI controller [9], [11], [18], otherwise the gains of that PI controller have to be increased notably to obtain a stable system.
- Cross control [17], [18] without diagonal coupling, $K_1 = K_4 = 0$: the outputs of the outer controllers are connected to the opposite current reference inputs as in the classic control structure. When a DC voltage disturbance occurs, the first reaction will be through the DC current. This will affect the energy, which will be compensated through the AC current. This structure improves the decoupling

between the AC and the DC sides, and appears to provide more consistent performance.

- Weighted control [18] for full (non-zero) coupling: this structure combines the two previous structures by connecting both PI outputs to both current reference inputs through four weighting factors, affecting the two current references at the same time. In this approach, the control system is provided with two extra degrees of freedom, obtaining six degrees of freedom overall (the $k_p - k_i$ ratio for both PI, and the four scaling factors).

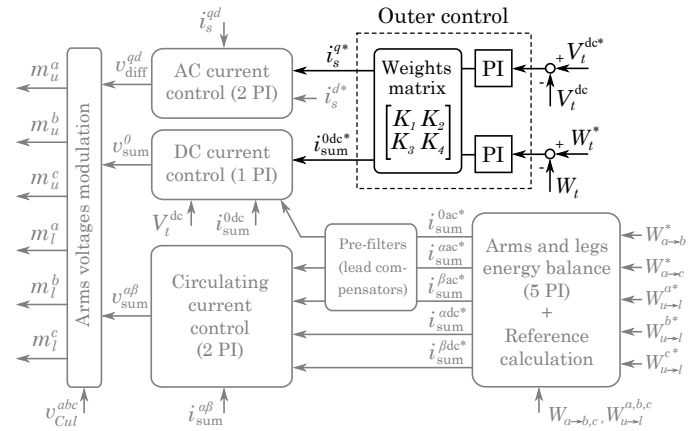


Fig. 3. Overall control scheme of a master MMC that unifies the standard control structures (classic, cross and weighted).

B. Standard tuning methods and their shortcomings

Typically the DC voltage control is tuned using a reference tracking rule used for tuning 2L-VSCs. This approach uses the DC capacitor as the plant and calculates the PI parameters based on a second-order characteristic polynomial

$$k_P = 2\xi\omega_n C_{dc}, \quad k_I = \omega_n^2 C_{dc}, \quad (5)$$

where ξ is the damping factor, ω_n is the natural frequency, and C_{dc} denotes the equivalent DC capacitance. However, the MMC does not contain a large physical DC capacitance, resulting in unsatisfactory DC voltage dynamic performance under DC power changes when this tuning rule is used [18]. While this tuning results in acceptable performance for HVDC links of several hundreds of kilometers, it is not obvious how to choose adequate gains for medium and short links.

For the energy controller, a disturbance rejection problem can be formulated and solved through a loop shaping strategy with a maximum allowed error and a specific settling time [9]. As the equivalent internal MMC capacitance is relatively big and independent of the link length, the controller performance is acceptable using this method. These tuning methods, however, are based on the assumption that the subsystems are isolated Single-Input Single-Output (SISO) systems, which is not necessarily true for MMCs.

C. Performance analysis of the different control structures

Next, we consider a point-to-point symmetrical monopole HVDC link (see Fig. 4) with a 25 km cable and apply the

mentioned tuning rules to the different control structures discussed in Section III-A. Figure 5 shows an AC power reference change in the slave converter from 0 to 1 p.u. at $t = 0.1$ s and from 1 p.u. to 0 at $t = 0.25$ s. The time-domain simulations have been performed using a full non-linear model in MATLAB Simulink, including (for both converters) the dynamics of the six arms, the vertical and horizontal energy balancing controllers, the saturation of the modulation indexes between 0 and 1 (half-bridge submodules), and the saturation of the current references. The parameters of the MMCs, the cable, and the controllers are summarized in Appendix A (Table I, Table II, and Table III). The tuning of the other controllers of the system (AC power, currents, PLL and energy balancing) is also briefly described in Appendix A. The cross

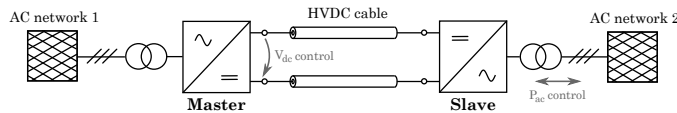


Fig. 4. Point-to-point symmetrical monopole HVDC link used as benchmark case study.

control shows a significant performance improvement over the classic structure. The only advantage of the classic structure is that the deviation of the energy is lower. The combined weighted structure acts on i_s^{q*} faster than the cross control, and also acts on i_{sum}^{0dc*} faster than the classic control. It is capable of compensating faster for energy deviations than the two other control structures. However, the AC and DC voltages show a slightly worse performance than the cross control structure after the second disturbance. Overall it can be seen that the combined (i.e., the weighted) structure offers flexibility in terms of dynamic performance of the different variables, as different weights can be set accordingly. The main challenge, however, lies on how to select the control gains and weights to achieve the desired control objectives. The results shown in Fig. 5 motivate the idea of a general Multi-Input Multi-Output (MIMO) outer control structure and a joint tuning method that accounts for the dynamics of the entire system and generalizes and improves upon the different standard control structures.

IV. GENERALIZED MIMO CONTROL STRUCTURE AND MODEL-BASED TUNING PROCEDURE

A. Proposed control structure

In this work, we propose a generalized multivariable outer control structure that consists of a 2×2 MIMO PI controller (Fig. 6) and subsumes the classic, cross, and weighted control structures. As in the weighted control, the current references i_s^{q*} and i_{sum}^{0dc*} are computed as a combination of the DC voltage (V_t^{dc}) and the total energy (W_t). The difference, however, is that this novel structure offers eight degrees of freedom that can be interpreted as parameters of four independent PI controllers: four $k_p - k_i$ ratios and four scaling gains. Instead, in the case of the weighted control only six degrees of freedom are obtained: two $k_p - k_i$ ratios and four scaling gains (Fig. 6). It is worth noting that the order of this new MIMO controller is actually the same as in the previous structures.

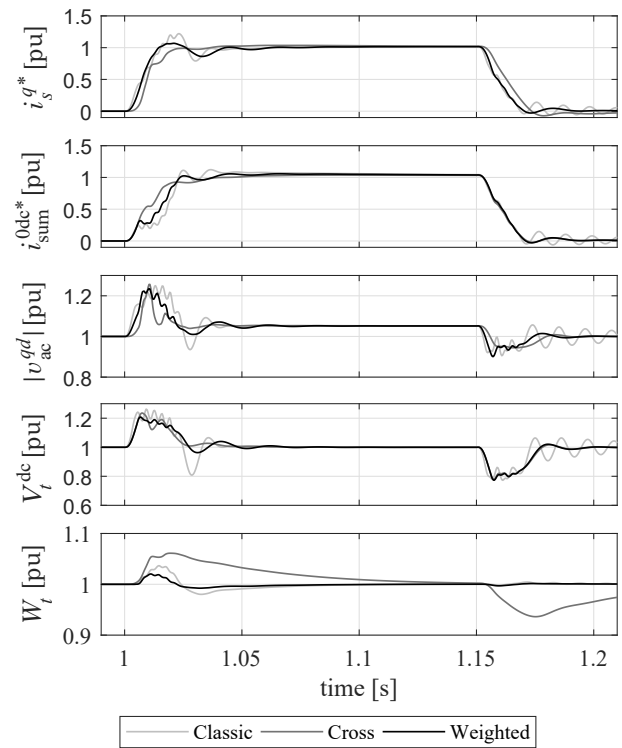


Fig. 5. Dynamic performance of the master MMC relevant magnitudes –Test case of a 25 km link.

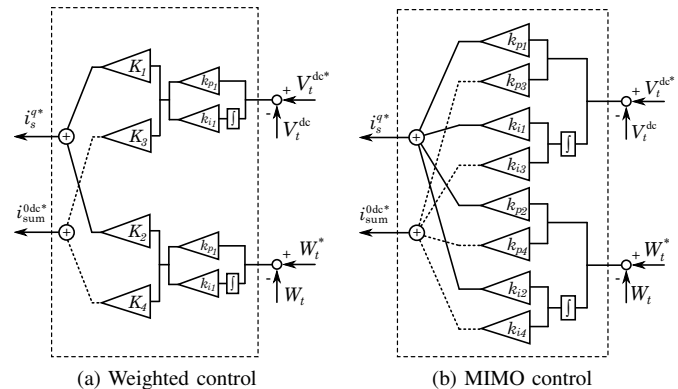


Fig. 6. Weighted and MIMO control structures comparison.

B. Derivation of a linear model

In order to perform linear analysis and apply our model-based tuning procedures we require a linear steady-state time-invariant (SSTI) model of the system.

1) *MMC linear model*: Capturing the overall MMC dynamics without simplifications in an SSTI model is a challenging problem by itself [21]. The main obstacle is that the circulating currents contain DC and several AC components at the same time. An extensive mathematical manipulation using a set of Synchronous Rotating Frames (SRF) at different frequencies can be performed [23]. However, this comes at the expense of having a large and complex model.

Nevertheless, the system can be re-formulated to enable the derivation of an SSTI model that uses energies as state variables instead of the voltages (4). This approach is suitable if an energy-based (CM) control approach is used [12]. This

formulation typically only considers the total energy and the circulating current zero-sequence component [15] and was recently generalized to include the arm balancing dynamics [12]. It is shown in [12] that the simplified model from [15] is suitable from a macroscopic point of view, and effectively captures the AC and DC dynamics, assuming that the internal vertical and horizontal energy balancing control are properly tuned. The tuning of the MMC's internal energy balancing controllers is typically only relevant in scenarios such as unbalanced AC voltage sags or DC pole imbalances. As this paper does not deal with such scenarios, we use a simplified linear model of the overall energy dynamics. To this end, we reformulate (4) into

$$\frac{dW_t}{dt} = -\frac{3}{2}v_{\text{diff}}^{qd}i_s^{qd} + 3i_{\text{sum}}^{0dc}v_{\text{sum}}^{0dc} \quad (6)$$

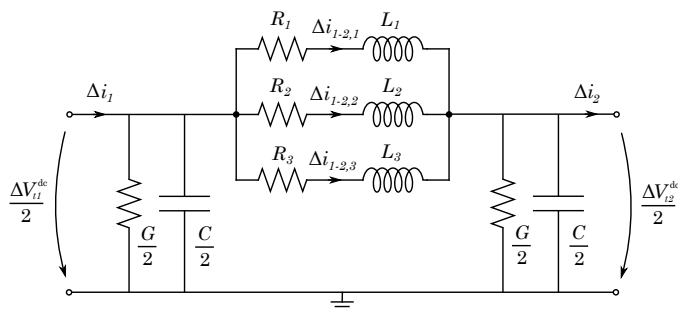
Expressing (2) in Park coordinates, reducing (3) to the zero-sequence component, linearizing (6), linearizing the PLL [18], and using the control scheme from Fig. 6, a linear SSTI model for a master MMC is obtained. Please see Appendix B for further details on the linearization procedure. In this model, the state and input vectors $\Delta x_{\text{MMC}} \in \mathbb{R}^{11}$ and $\Delta u_{\text{MMC}} \in \mathbb{R}^6$ are given by

$$\begin{aligned} \Delta x_{\text{MMC}} &= (\Delta \zeta_{\text{pll}}^{12}, \Delta i_s^{qd}, \Delta i_{\text{sum}}^{0dc}, \Delta W_t, \Delta \gamma_s^{qd}, \Delta \xi_{\text{sum}}^0, \Delta \sigma_v, \Delta \kappa_w) \\ \Delta u_{\text{MMC}} &= (\Delta V_t^{\text{dc}*}, \Delta W_t^*, \Delta V_t^{\text{dc}}, \Delta Q_{\text{ac}}^*, \Delta v_g^{qd}), \end{aligned} \quad (7)$$

where $\Delta \zeta_{\text{pll}}^{12}$ are the two integral states related to the PLL dynamics; $\Delta \gamma_s^{qd}$ are the two integral states related to the i_s^{qd} controllers; $\Delta \xi_{\text{sum}}^0$ is the integral state related to the i_{sum}^{0dc} controller; and $\Delta \sigma_v$ and $\Delta \kappa_w$ are the integral states of the multivariable outer controller (related to V_t^{dc} and W_t).

2) *Linear cable model:* The lumped parameter model with parallel branches from [24] is considered. In contrast to the classic π -section, this model represents the frequency-dependent behavior of the cable. In the present study, three branches and one section have been used (see Fig. 7), based on the data from [21], which accurately represents the behaviour of the cable up to a few hundreds of Hz. The differential equations for three parallel branches and an arbitrary number of sections can be found in [18]. The corresponding states $\Delta x_{\text{cable}} \in \mathbb{R}^5$ and inputs $\Delta u_{\text{cable}} \in \mathbb{R}^2$ are given by

$$\begin{aligned} \Delta x_{\text{cable}} &= (\Delta V_{t1}^{\text{dc}}, \Delta i_{1-2,1}, \Delta i_{1-2,2}, \Delta i_{1-2,3}, \Delta V_{t2}^{\text{dc}}), \\ \Delta u_{\text{cable}} &= (\Delta i_1, \Delta i_2). \end{aligned} \quad (8)$$



3) *Overall linear system model:* The linear model of the overall system is obtained by interconnecting the models of the MMCs and the cable through the DC voltage V_t^{dc} (see Fig. 8). To reduce the model order we focus on the master converter and model the slave converter as a controlled DC current source with a first-order low-pass filter (extra state $\Delta x_{\text{slave}} \in \mathbb{R}$) modeling its response time. The time constant of the low-pass filter is equivalent to the time constant of the slave converter AC power loop (τ_p). Then, the state space of the overall linear system is defined by $\Delta x \in \mathbb{R}^{17}$ and $\Delta u \in \mathbb{R}^6$ given by

$$\begin{aligned} \Delta x_{\text{overall}} &= (\Delta x_{\text{MMC}}, \Delta x_{\text{cable}}, \Delta x_{\text{slave}}), \\ \Delta u_{\text{overall}} &= (\Delta V_t^{\text{dc}*}, \Delta W_t^*, \Delta Q_{\text{ac}}^*, \Delta v_g^{qd}, \Delta P_2^*). \end{aligned} \quad (9)$$

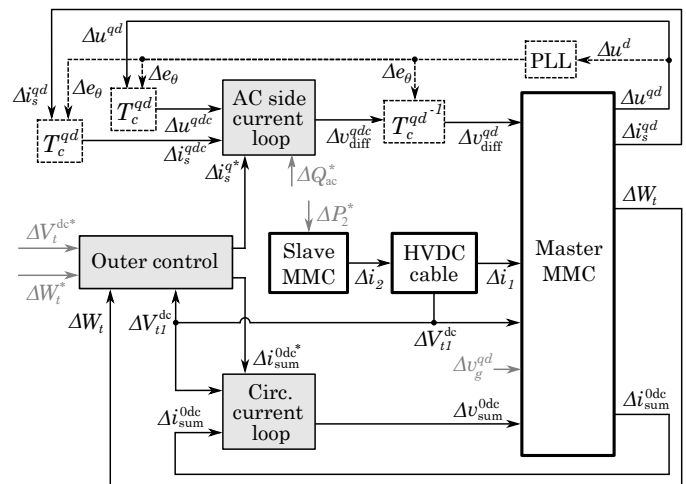


Fig. 7. Lumped parameter cable model, with one section and three branches corresponding to one monopole.

Fig. 8. Block diagram of the overall linear system model. The input signals are shown in gray color.

Moreover, the inputs $\Delta V_t^{\text{dc}*}$, ΔQ_{ac}^* , ΔW_t^* and Δv_g^{qd} are not considered as disturbances in the present study, so they are set to zero in the small-signal model. The only disturbance considered is the AC power reference of the slave converter (ΔP_2^*), which is divided by the nominal voltage $\Delta V_t^{\text{dc}*}$ and, after passing through the first-order filter that emulates the slave converter dynamics, yields the current Δi_2 . Then, the closed-loop system can be described by the following equations (see Fig. 9)

$$\begin{cases} \Delta \dot{x} = \mathbf{A}\Delta x + \mathbf{B}\Delta u + \mathbf{G}\Delta w \\ \Delta u = \mathbf{F}\Delta y \\ \Delta y = \mathbf{C}\Delta x \\ \Delta z = \tilde{\mathbf{C}}\Delta x + \tilde{\mathbf{D}}\Delta u \end{cases}, \quad (10)$$

where $\Delta w \in \mathbb{R}$ denotes the disturbance input accounting for the DC current of the slave converter, $\Delta y \in \mathbb{R}^8$ are the measured outputs to be regulated, $u \in \mathbb{R}^8$ denotes the control inputs, and $\Delta z \in \mathbb{R}^3$ denotes the physical performance output

of interest to quantify performance:

$$\begin{aligned}\Delta w &= \Delta P_2^*, \\ \Delta y &= (\Delta e_v, \Delta \sigma_v, \Delta e_w, \Delta \kappa_w, \Delta e'_v, \Delta \sigma'_v, \Delta e'_w, \Delta \kappa'_w), \\ \Delta u &= (\Delta i_v^P, \Delta i_v^I, \Delta i_w^P, \Delta i_w^I, \Delta i_v^{P'}, \Delta i_v^{I'}, \Delta i_w^{P'}, \Delta i_w^{I'}), \\ \Delta z &= (\Delta v_{\text{diff}}^q, \Delta W_t, \Delta V_t^{\text{dc}}).\end{aligned}$$

The vector Δy contains the DC voltage deviation and its integral, i.e., $(\Delta e_v, \Delta \sigma_v, \Delta e'_v, \Delta \sigma'_v)$ as well as the deviation of the total energy and its integral $(\Delta e_w, \Delta \kappa_w, \Delta e'_w, \Delta \kappa'_w)$, and the vector Δu contains the proportional (P) and integral (I) components of the reference currents. The ' symbol refers to the control efforts of the second output reference ($i_{\text{sum}}^{\text{0dc}*}$). For clarity of the presentation, only the three most important performance outputs have been selected for the physical performance output vector Δz .

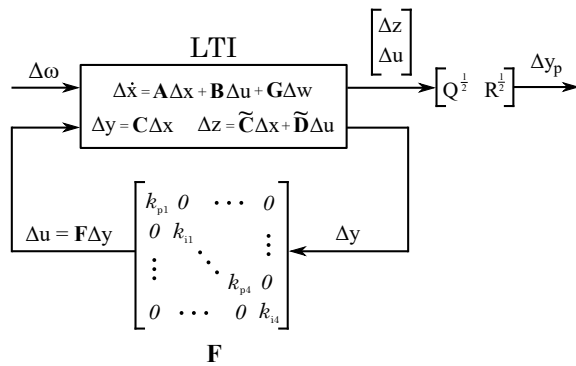


Fig. 9. Closed-loop standard form of the overall linear model.

C. \mathcal{H}_2 -norm optimization for optimal tuning

The control gains of the MIMO control system (i.e., the parameters in the matrix F) are tuned by optimizing the \mathcal{H}_2 -norm [25]–[27] of the system. Broadly speaking, the \mathcal{H}_2 -norm provides a measure of the magnitude of a weighted performance output vector Δy_p in response to a disturbance input vector Δw . The \mathcal{H}_2 -norm has several (equivalent) interpretations. It captures the energy of the output signals Δy_p in response to impulsive disturbances, it measures the rate of change of the output energy for a step disturbance, and it captures the variance of Δy_p in response to white noise. In a power system this can be interpreted as a line opening/closing (impulse), load-step or loss of a generator (step), and fluctuations of renewable generation (white noise). Moreover, in frequency domain, minimizing the \mathcal{H}_2 -norm corresponds to a minimization of the area under the magnitude plot of the Bode diagram.

To apply \mathcal{H}_2 -norm optimization to the tuning problem at hand, we first define a performance output Δy_p that contains the outputs of interest (i.e., Δz) as well as positive (semi)definite matrices \mathbf{Q} and \mathbf{R} that penalize the deviation of the performance outputs Δz and the control effort Δu :

$$\Delta y_p = \mathbf{Q}^{\frac{1}{2}} \tilde{\mathbf{C}} \Delta x + \mathbf{Q}^{\frac{1}{2}} \tilde{\mathbf{D}} \Delta u + \mathbf{R}^{\frac{1}{2}} \Delta u \quad (11)$$

For clarity of the presentation we defined the weighted performance output Δy_p using the physical performance output

Δz , whereas the standard approach in the control literature directly uses \mathbf{Q} and \mathbf{R} to define the output Δz in (10). The performance output is used to formulate the cost function:

$$\begin{aligned}J_\infty &= \int_0^\infty y_p^\top y_p dt, \\ &= \int_0^\infty \Delta x^\top \tilde{\mathbf{C}}^\top \mathbf{Q} \tilde{\mathbf{C}} \Delta x + \Delta u^\top (\tilde{\mathbf{D}}^\top \mathbf{Q} \tilde{\mathbf{D}} + \mathbf{R}) \Delta u dt\end{aligned}$$

The complete dynamical system \mathcal{G} is obtained by closing the loop via $\Delta u = F\Delta y$ as in Fig. 9 and using (11):

$$\begin{aligned}\Delta \dot{x} &= (\mathbf{A} + \mathbf{BFC})\Delta x + \mathbf{G}\Delta w = \mathbf{A}_{\text{cl}}\Delta x + \mathbf{G}\Delta w \\ \Delta y_p &= (\mathbf{Q}^{\frac{1}{2}} \tilde{\mathbf{C}} + \mathbf{Q}^{\frac{1}{2}} \tilde{\mathbf{D}}\mathbf{FC} + \mathbf{R}^{\frac{1}{2}} \mathbf{FC})\Delta x = \mathbf{C}_{\text{cl}}\Delta x\end{aligned}$$

Even though the \mathcal{H}_2 -norm does not explicitly optimize time-domain criteria (such as the overshoot), it can be used to obtain adequate time-domain performance. The optimization problem to be solved is defined by [27]

$$\min_F \|\mathcal{G}\|_2^2 \quad (x_{\min} < x < x_{\max}) \quad (12)$$

The \mathcal{H}_2 -norm between the disturbance input Δw and the performance output y_p is given by [26]

$$\|\mathcal{G}\|_2^2 = \text{trace}(\mathbf{G}^\top \mathbf{P}_F \mathbf{G}) \quad (13)$$

where \mathbf{P}_F is the closed-loop observability Gramian obtained as positive definite solution of the Lyapunov equation

$$\mathbf{P} \mathbf{A}_{\text{cl}} + \mathbf{A}_{\text{cl}}^\top \mathbf{P} + \mathbf{C}_{\text{cl}}^\top \mathbf{C}_{\text{cl}} = 0 \quad (14)$$

for a fixed \mathbf{F} . Due to the structure imposed on \mathbf{F} (see Fig. 9), the optimization problem (12) is generally non-convex. However, it can be solved efficiently by noting that the gradient of $\|\mathcal{G}\|_2^2$ with respect to the control gains can be computed efficiently. The gradient computation used in [27] cannot be applied here, because \mathbf{C}_{cl} also depends on the control gains. Therefore, we use steps similar to the ones in [28] to derive an expression for the gradient of $\|\mathcal{G}\|_2^2$ that requires computing the observability Gramian (i.e., (14)) and controllability Gramian, i.e., that requires the solution of two Lyapunov equations. The details are omitted for reasons of space. Finally, we remark that our approach can be used to optimize the control parameters for multiple operating points by considering the sum of the \mathcal{H}_2 -norms at different linearization points (but with the same control parameters) as cost function. However, for the sake of clarity, we consider a single operating point in this study.

V. CASE STUDY

In this section, we apply the \mathcal{H}_2 -norm optimization to tune the control gains of the master converter MIMO control structure. First, we study the sensitivity of the performance outputs with respect to the penalty parameters. Next, we iteratively update the penalties to obtain optimal control gains and validate the resulting control performance using the full non-linear model described in Section III (Fig. 4) applying an AC power reference change in the slave converter from 0 to 1 p.u. (i.e., flowing from the slave to the master) at $t = 0.2$ s. This relatively large disturbance is a suitable benchmark scenario to verify the effectiveness of the proposed method. Two different scenarios are considered:

- Case 1: Short link of 50 km. Examples of similar real-world projects are Cross-Sound (USA, 40 km, 2002), INELFE (Spain-France, 65 km, 2015), and ElekLink (UK-France, 51 km, to be commissioned in 2020).
- Case 2: Very short link of 5 km. A potential application of a such a short link is the interconnection of neighboring systems, either at different frequencies or simply non-synchronous. An example of an already existing very short cable project is the Xiamen Island VSC-HVDC demonstrator (China, 10.7 km, 2015).

The \mathcal{H}_2 -norm approach presented in the previous is implemented in MATLAB using the SQP algorithm of `fmincon` and applied to a linear model corresponding to an operating point given by a DC power flow of 1 p.u. from the slave to the master converter. Furthermore, the tuning rules discussed in Section III-B are used to obtain an initial guess for the control gains to warm-start the optimization.

A. Sensitivity with respect to performance penalties

One of the advantages of using an optimization method is that it allows for a more intuitive, principled, multivariable, and obviously optimal tuning procedure, i.e., instead of directly tuning the individual gains (eight in total) of SISO controllers, the focus is put on the penalties on the desired performance outputs (\mathbf{Q}) and control inputs (\mathbf{R}). We first study how the penalties correlate with time-domain performance. To this end, we focus on the AC voltage (v_{diff}^q), the total energy (W_t), and the DC voltage (V_t^{dc}) as the most relevant performance outputs that are penalized by the matrix

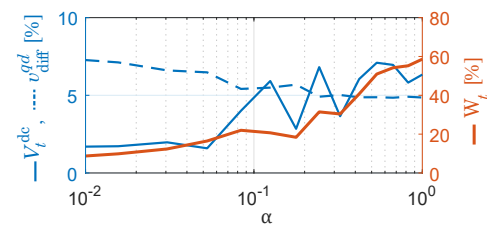
$$\mathbf{Q} = \text{diag}(q_{v_{\text{ac}}}, q_{w_t}, q_{v_{\text{dc}}}) \quad (15)$$

Moreover, the matrix \mathbf{R} penalizes the 8 control inputs $\Delta u = \mathbf{F}\Delta y$, where \mathbf{F} contains the tunable static gains.

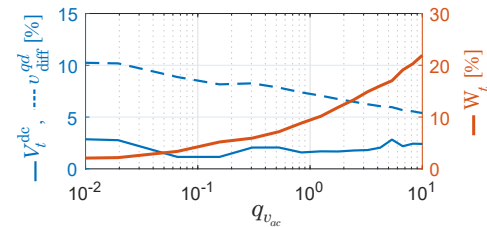
$$\mathbf{R} = \alpha \text{diag}(r_{p_1}, r_{i_1}, \dots, r_{p_4}, r_{i_4}) \quad (16)$$

As the system is normalized to a per unit framework, the initial guess for the penalties \mathbf{Q} and \mathbf{R} is the identity matrix. The effect of different penalties on the dynamics of the outputs of interest is shown in Fig. 10 using a cable of 10 km. First, looking at α (the $\mathbf{Q} - \mathbf{R}$ ratio) it can be seen that all magnitudes have low overshoot when this value is low. A value of $\alpha = 0.01$ is fixed for the next cases. Increasing the penalty on v_{diff}^q reduces the overshoot of the AC voltage but at the expense of increasing the overshoot of the total energy. On the other hand, increasing the penalty in W_t shows the opposite effect. Finally, increasing the penalty in V_t^{dc} reduces the overshoot of the DC voltage, even though this magnitude is already at a reasonable level in the previous cases using $\alpha = 0.01$.

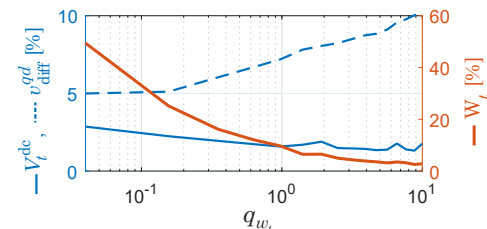
The results in Fig. 10 highlight how the control gains can be modified through the choice of penalties to achieve the desired performance. Analyzing time-domain metrics is a good way to receive feedback from the optimization, and allows for iterating the penalties until an acceptable result is found.



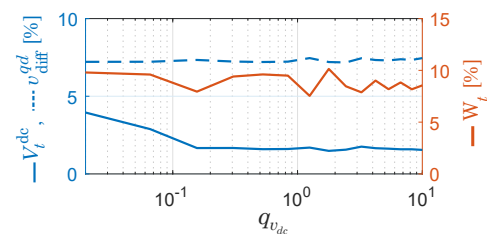
(a) Parametric sweep of α



(b) Parametric sweep of $q_{v_{\text{ac}}}$



(c) Parametric sweep of q_{w_t}



(d) Parametric sweep of $q_{v_{\text{dc}}}$

Fig. 10. Effect of different penalties –Overshoot of the DC voltage, AC voltage and total energy, in a 10 km link test case.

B. Results and discussion

Next, we use the insights on how the penalties affect the resulting performance and apply the \mathcal{H}_2 optimization to both Case 1 and Case 2. Both penalty matrices \mathbf{Q} and \mathbf{R} are initially set to the identity, and α is set to 0.01. Next, the penalties are modified in two iterations to obtain the desired dynamic performance. The resulting time-domain responses after every iteration are shown in Fig. 11. The initial tuning in the 50 km case is equivalent to the weighted control approach with $k_1 = k_2 = k_3 = k_4 = 1$ (see Table III in the Appendix A). In the 5 km case, the gains of $\text{PI}_1(s)$ and $\text{PI}_3(s)$ (i.e., the critical controller related to the DC voltage) are multiplied by a factor of 4 to obtain a stabilizing initial tuning.

The first iteration (i.e., with \mathbf{Q} and \mathbf{R} set to identity) results in a clear improvement of the initial tuning that avoids the converter saturation limits (see the magnitudes v_{diff}^q and V_t^{dc} in Fig. 11b). However, the deviation of W_t is relatively big. In order to address this issue, a penalty of $q_{w_t} = 3$ is used

in the second iteration, which shows a significant reduction of the deviation of W_t . However, W_t does not converge back to zero after the disturbance. This can also be seen in the Bode plots of W_t with respect to the input disturbance in Fig. 12 that remain at a relatively large value for low frequencies. Moreover, the optimization results in a very high gain k_{p3} (25 times higher than the initial tuning value in both Cases 1 and 2, see Fig. 13) that could compromise the stability of the full original non-linear system, since the operation condition is potentially far from the region where the linearized model is valid. The effects of high gain control can also be observed in the small overshoots of V_t^{dc} in Fig. 11 and in the left Bode plots in Fig. 12, which show that the curves are pushed down aggressively.

As discussed before (cf. Fig. 10a), a lower value in R results in a higher control effort. Therefore, in order to overcome the aforementioned issues, r_{i2} and r_{i4} are both reduced to 0.05 (50 km) and 0.01 (5 km) to increase the integral control effort related to the energy, and r_{p1} and r_{p3} are both increased to 50 (Case 1) and 100 (Case 2) to reduce the proportional control effort related to the DC voltage, aiming for a less aggressive controller. As a result, after this third iteration of the penalties, the energy reaches its reference value relatively fast, and k_{p3} is significantly reduced: 5.6 times higher than the initial tuning value in Case 1, and 10 times in Case 2, see Fig. 13. Accordingly, Fig. 11 shows that the DC voltage overshoot has increased, and the right Bode plots in Fig. 12 show that the curves are no longer flat at low frequencies. While these results have been obtained for a linearization point corresponding to a DC power flow of 1 p.u. from the slave to the master converter, the resulting control gains result in similar performance characteristics at other operating points (e.g., for a power flow of 1 p.u. from the master to the slave converter).

Based on this challenging case study we observe that:

- The standard tuning rules (based on SISO assumption) used in the MIMO control structure yield acceptable results for long cables (Fig. 11a). However, as discussed in Section III-B, they result in poor performance for shorter links (i.e., a more coupled and stressed system), e.g., resulting in big overshoots in the DC voltage.
- With the proposed method it is possible to automatically obtain an optimal tuning which outperforms the initial one – especially for short cables. Also, the penalties can be tuned in an intuitive way to prioritize the response of some converter outputs over others, depending on the desired specifications of voltages and internal energy.
- Surprisingly, the optimal control gains in the proposed MIMO control structure are negative in some cases (see $PI_4(s)$ in Fig. 13). While it may seem counter intuitive from a SISO control point of view, negative control gains can result in improved performance (rather than instability) in a MIMO control structure. Specifically, due to the fact that two different signals participate in each of the control outputs, the combination of positive and negative control efforts can lead to a better solution. Nonetheless, if needed, the control gains can be constrained to positive values in the optimization routine.

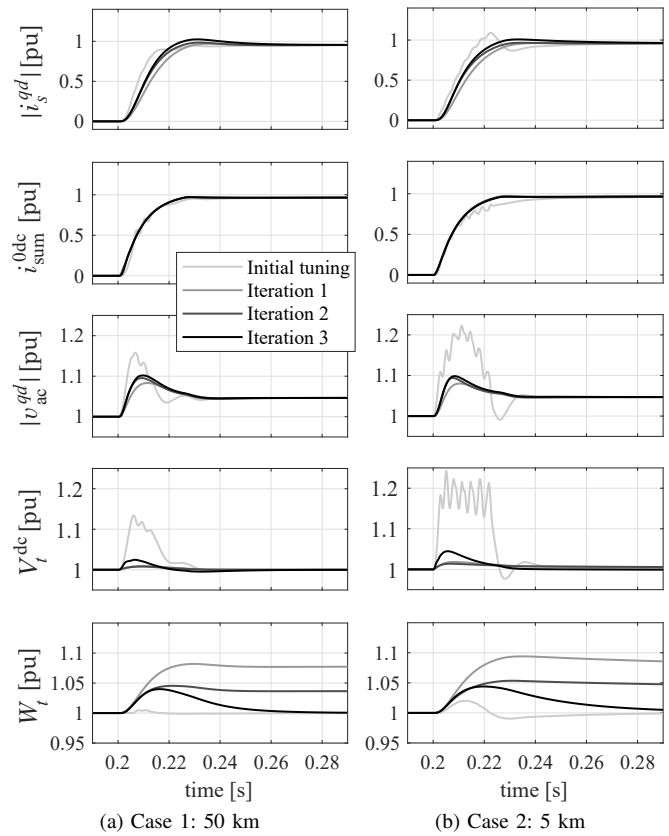


Fig. 11. Time-domain simulation results –Initial tuning is identical to the weighted control structure in Fig. 5, and Iterations 1 to 3 correspond to different penalties in the \mathcal{H}_2 -norm optimization.

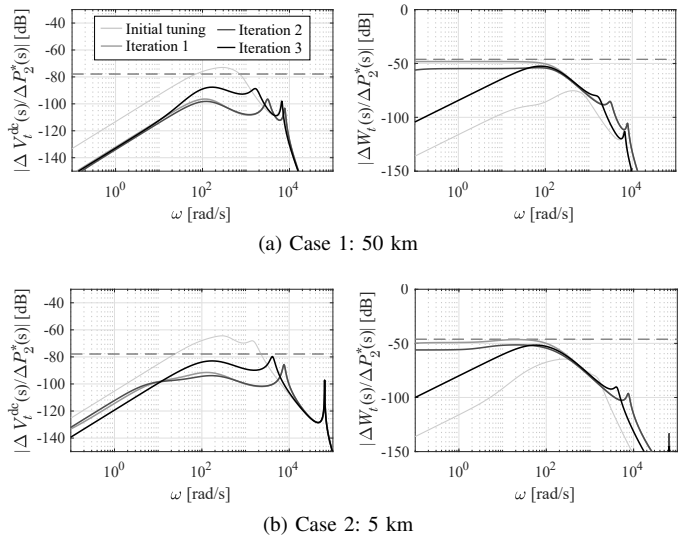


Fig. 12. Bode magnitude plots –DC voltage and energy of the master MMC, for the initial tuning and the \mathcal{H}_2 tuning (three iterations changing the penalties). Horizontal dashed gray line corresponds to a 10% error of the corresponding magnitude.

VI. CONCLUSIONS

A generalized MIMO outer control structure for a master MMC, using the DC voltage and the internal energy as inputs and the AC and DC current references as outputs, has been presented that subsumes several well-known control structures for MMCs as special cases. Rather than explicitly

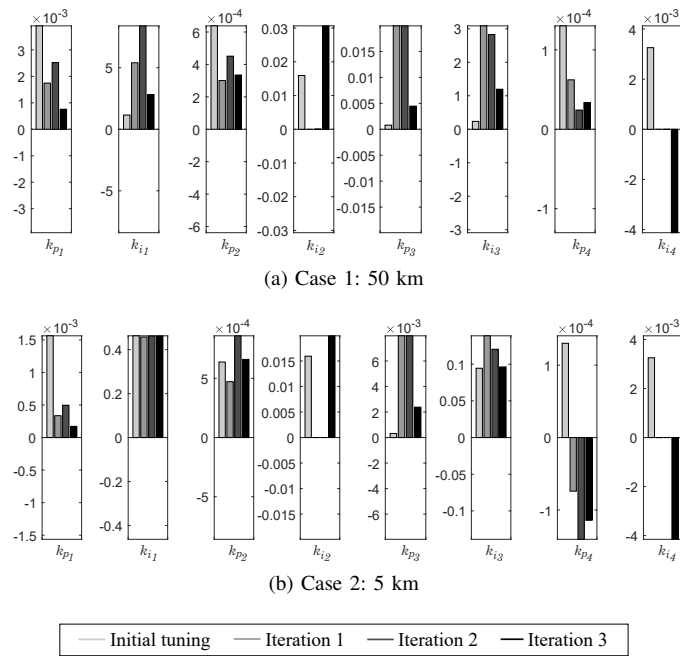


Fig. 13. MIMO controller \mathcal{H}_2 tuning results –Parameters k_p and k_i of the initial tuning and the \mathcal{H}_2 tuning (three iterations changing the penalties).

tuning the eight control parameters of this generalized MIMO outer control, which would be complex and non-intuitive, a systematic model-based tuning methodology, based on the \mathcal{H}_2 -norm, is proposed that allows for intuitive tuning of the controls through penalty factors on performance outputs. An improvement of the overall dynamic performance of the MMC has been obtained, especially in low DC inertia scenarios arising from short and very short HVDC links, in which guidelines for manual control tuning break down. Moreover, as the proposed methodology allows the penalization of the disturbance response of different performance outputs, as well as the control efforts, it results in a flexible tuning method. In particular, different control objectives such as tight DC voltage regulation, minimization of internal energy deviations, and the efficient use of control energy can be intuitively combined and different trade-offs are easily established by changing the penalties. This approach allowed us to reduce the overshoot of the DC voltage in critically short cable cases, and to iteratively improve the tuning of the integral control action of the controller to ensure that the internal energy reaches the desired steady-state (i.e., zero error) sufficiently fast.

APPENDIX A

PARAMETERS OF THE SYSTEM AND TUNING RULES

System parameters and initial tuning are shown in Tables I-III. The following parameters are set: $\omega_n = 2\pi/(15\tau_{cc})$, $\xi = 0.707$, $C_{dc} = c/2 d_{link}$ (d_{link} : length of the link), and $k_1 = k_2 = k_3 = k_4 = 1$. The other PI controllers of the system are tuned according to the following well-known rules [18]:

- AC power loop (only slave MMC): set-point tracking (first-order closed-loop response of $\tau_p = 10$ ms).

- AC grid and circulating current controllers: Internal Model Control (first-order closed-loop response of $\tau_{cc} = 1$ ms).
- PLL: grid angle tracking in approximately 20 ms.
- Horizontal balancing energy controllers:
 $k_p = 1/(3V_N^{dc})$ 25, $k_i = 1/(3V_N^{dc})$ 625.
- Vertical balancing energy controllers:
 $k_p = -\sqrt{2}/(\sqrt{3}U_N)$ 25, $k_i = -\sqrt{2}/(\sqrt{3}U_N)$ 625.

TABLE I
MMC AND AC GRID PARAMETERS [9], [18]

Parameter	Symbol	Value	Units
Rated (base) active power	P_N	500	MW
Rated (base) AC-side voltage	U_N	320	kV
Rated (base) DC-side voltage	V_N^{dc}	± 320	kV
Grid short-circuit ratio	SCR	10	-
Coupling impedance	$R_s + jL_s$	0.01+j0.2	pu
Arm reactor impedance	$R_a + jL_a$	0.01+j0.2	pu
Converter submodules per arm	N_{arm}	400	-
Average submodule voltage	V_{SM}	1.6	kV
Submodule capacitance	C_{SM}	8	mF

TABLE II
CABLE PARAMETERS (SINGLE MONOPOLE) [21]

Symbol	Value	Units	Symbol	Value	Units
r_1	0.1265	Ω/km	l_1	0.2644	mH/km
r_2	0.1504	Ω/km	l_2	7.2865	mH/km
r_3	0.0178	Ω/km	l_3	3.6198	mH/km
c	0.1616	$\mu\text{F}/\text{km}$	g	0.1015	$\mu\text{S}/\text{km}$

TABLE III
DC VOLTAGE AND ENERGY PI CONTROLLERS INITIAL TUNING VALUES

K_1	K_2	K_3	K_4
$-\sqrt{2}V_N^{dc}k_1/(\sqrt{3}U_N)$	$-\sqrt{2}k_2/(\sqrt{3}U_N)$	$-k_3/3$	$k_4/(3V_N^{dc})$

	PI ₁ (s)	PI ₂ (s)	PI ₃ (s)	PI ₄ (s)
k_p	$K_1 2\xi\omega_n C_{dc}$	$K_2 250$	$K_3 2\xi\omega_n C_{dc}$	$K_4 250$
k_i	$K_1 \omega_n^2 C_{dc}$	$K_2 6250$	$K_3 \omega_n^2 C_{dc}$	$K_4 6250$

APPENDIX B LINEARIZATION

By linearizing the energy equation (6) we obtain:

$$\Delta \dot{W}_t = -\frac{3}{2}(\Delta v_{diff}^q i_{s0}^q + \Delta v_{diff}^d i_{s0}^d + \Delta i_s^q v_{diff0}^q + \Delta i_s^d v_{diff0}^d) + 3(\Delta i_{sum}^{0dc} v_{sum0}^{0dc} + \Delta v_{sum}^{0dc} i_{sum0}^{0dc}).$$

Moreover, the error of the angle deviation due to PLL dynamics can be modelled as:

$$\Delta e_\theta = -\frac{k_{p-pll}s + k_{i-pll}}{s^2 + u_0^q k_{p-pll}s + u_0^q k_{i-pll}} \Delta u^d. \quad (17)$$

This angle error is used to transform magnitudes between the converter reference (x^{qdc}) and the grid reference (x^{qd}) [29]. Next, we define

$$\mathbf{T}_c^{qd} = \begin{bmatrix} \cos(e_{\theta_0}) & -\sin(e_{\theta_0}) & -\sin(e_{\theta_0})x_0^q - \cos(e_{\theta_0})x_0^d \\ \sin(e_{\theta_0}) & \cos(e_{\theta_0}) & \cos(e_{\theta_0})x_0^q - \sin(e_{\theta_0})x_0^d \end{bmatrix} \quad (18)$$

$$\mathbf{T}_c^{qd^{-1}} = \begin{bmatrix} \cos(e_{\theta_0}) & \sin(e_{\theta_0}) & -\sin(e_{\theta_0})x_0^q + \cos(e_{\theta_0})x_0^d \\ -\sin(e_{\theta_0}) & \cos(e_{\theta_0}) & -\cos(e_{\theta_0})x_0^q - \sin(e_{\theta_0})x_0^d \end{bmatrix} \quad (19)$$

and use the transformation

$$\Delta x^{qdc} = \mathbf{T}_c^{qd}(\Delta x^{qd}, \Delta e_\theta)^T \quad (20)$$

to obtain the feedback variables i_s^{qdc} and u^{qdc} , whereas the inverse transformation

$$\Delta x^{qd} = \mathbf{T}_c^{qd^{-1}}(\Delta x^{qdc}, \Delta e_\theta)^T \quad (21)$$

is used to transform the controller output v_{diff}^{qdc} into v_{diff}^{qd} .

REFERENCES

- [1] D. Van Hertem, O. Gomis-Bellmunt, and J. Liang, *HVDC grids: for offshore and supergrid future*, ser. IEEE Press Series on Power Engineering. Wiley, 2016.
- [2] A. Lesnicar and R. Marquardt, "An innovative modular multilevel converter topology suitable for a wide power range," in *IEEE PowerTech*, vol. 3, 2003, pp. 272–277.
- [3] R. Adapa, "High-Wire Act. HVdc technology: The State of the Art," *IEEE Power Energy Mag.*, pp. 18–29, 2012.
- [4] Q. Tu, Z. Xu, and L. Xu, "Reduced Switching-frequency modulation and circulating current suppression for modular multilevel converters," *IEEE Trans. Power Del.*, vol. 26, no. 3, pp. 2009–2017, 2011.
- [5] L. Angquist, A. Antonopoulos, D. Siemaszko, K. Ilves, M. Vasiladiotis, and H.-P. Nee, "Open-loop control of modular multilevel converters using estimation of stored energy," *IEEE Trans. Ind. Appl.*, vol. 47, no. 6, pp. 2516–2524, 2011.
- [6] L. Harnefors, A. Antonopoulos, S. Norrga, L. Angquist, and H. P. Nee, "Dynamic analysis of modular multilevel converters," *IEEE Trans. Ind. Electron.*, vol. 60, no. 7, pp. 2526–2537, 2013.
- [7] A. J. Far and D. Jovicic, "Small-Signal Dynamic DQ Model of Modular Multilevel Converter for System Studies," *IEEE Trans. Power Del.*, vol. 31, no. 1, pp. 191–199, 2016.
- [8] G. Bergna, J. A. Suul, and S. D'Arco, "State-space modelling of modular multilevel converters for constant variables in steady-state," in *IEEE Workshop on Control and Modeling for Power Electronics (COMPEL)*, 2016.
- [9] E. Prieto-Araujo, A. Junyent-Ferré, C. Collados-Rodríguez, G. Clariana-Colet, and O. Gomis-Bellmunt, "Control design of Modular Multilevel Converters in normal and AC fault conditions for HVDC grids," *Electr. Power Syst. Res.*, vol. 152, pp. 424–437, 2017.
- [10] A. Antonopoulos, L. Angquist, and H.-P. Nee, "On dynamics and voltage control of the Modular Multilevel Converter," in *European Conference on Power Electronics and Applications (EPE)*, 2009.
- [11] J. Freytes, S. Akkari, J. Dai, F. Gruson, P. Rault, and X. Guillaud, "Small-signal state-space modeling of an HVDC link with modular multilevel converters," in *IEEE Workshop on Control and Modeling for Power Electronics (COMPEL)*, 2016.
- [12] G. Bergna-Diaz, J. A. Suul, and S. D'Arco, "Energy-Based State-Space Representation of Modular Multilevel Converters with a Constant Equilibrium Point in Steady-State Operation," *IEEE Trans. Power Electron.*, vol. 33, no. 6, pp. 4832–4851, 2018.
- [13] K. Sharifabadi, L. Harnefors, H. Nee, S. Norrga, and R. Teodorescu, *Design, Control, and Application of Modular Multilevel Converters for HVDC Transmission Systems*, ser. Wiley - IEEE. Wiley, 2016.
- [14] J. Freytes, G. Bergna, J. A. Suul, S. D'Arco, F. Gruson, F. Colas, H. Saad, and X. Guillaud, "Improving Small-Signal Stability of an MMC with CCSC by Control of the Internally Stored Energy," *IEEE Trans. Power Del.*, vol. 33, no. 1, pp. 429–439, 2018.
- [15] G. Bergna Diaz, J. A. Suul, and S. D'Arco, "Small-signal state-space modeling of modular multilevel converters for system stability analysis," in *IEEE Energy Conversion Congress and Exposition (ECCE)*, 2015, pp. 5822–5829.
- [16] K. Shinoda, A. Benchaib, J. Dai, and X. Guillaud, "Virtual Capacitor Control: Mitigation of DC Voltage Fluctuations in MMC-Based HVdc Systems," *IEEE Trans. Power Del.*, vol. 33, no. 1, pp. 455–465, 2018.
- [17] G. Bergna, J. A. Suul, and S. D'Arco, "Impact on small-signal dynamics of using circulating currents instead of AC-currents to control the DC voltage in MMC HVDC terminals," in *IEEE Energy Conversion Congress (ECCE)*, 2016.
- [18] E. Sánchez-Sánchez, E. Prieto-Araujo, A. Junyent-Ferré, and O. Gomis-Bellmunt, "Analysis of MMC Energy-based Control Structures for VSC-HVDC Links," *IEEE Trans. Emerg. Sel. Topics Power Electron.*, vol. 6, no. 3, pp. 1065–1076, 2018.
- [19] H. Saad, S. Denmetiere, J. Mahseredjian, P. Delarue, X. Guillaud, J. Peralta, and S. Nguéfeu, "Modular multilevel converter models for electromagnetic transients," *IEEE Trans. Power Del.*, vol. 29, no. 3, pp. 1481–1489, 2014.
- [20] C. E. Ugalde-Loo, O. D. Adeuyi, S. Eang, N. Jenkins, S. Ceballos, M. Santos, I. Vidaurrazaga, S. D'Arco, G. Bergna, M. Barenys, M. Parker, S. Finney, A. Gatti, A. Pitto, M. Rapizza, D. Cirio, P. Lund, A. Castro, and I. Azpiri, "Open access simulation toolbox for the grid connection of offshore wind farms using multi-terminal HVDC networks," in *IET International Conference on AC and DC Power Transmission*, 2017.
- [21] J. Freytes, "Small-signal stability analysis of Modular Multilevel Converters and application to MMC-based Multi-Terminal DC grids," Ph.D. dissertation, Ecole Centrale de Lille, 2017.
- [22] S. Debnath, J. Qin, B. Bahrani, M. Saeedifard, and P. Barbosa, "Operation, Control, and Applications of the Modular Multilevel Converter: A Review," *IEEE Trans. Power Electron.*, vol. 30, no. 1, pp. 37–53, 2014.
- [23] G. Bergna-Diaz, J. Freytes, X. Guillaud, S. D'Arco, and J. A. Suul, "Generalized Voltage-based State-Space Modelling of Modular Multilevel Converters with Constant Equilibrium in Steady-State," *IEEE Trans. Emerg. Sel. Topics Power Electron.*, vol. 6, no. 2, pp. 707–725, 2018.
- [24] J. Beerten, S. D'Arco, and J. A. Suul, "Frequency-dependent cable modelling for small-signal stability analysis of VSC-HVDC systems," *IET Generation, Transmission & Distribution*, vol. 10, no. 6, pp. 1370–1381, 2016.
- [25] S. Skogestad and I. Postlethwaite, *Multivariable feedback control: analysis and design*. Wiley, 2005.
- [26] K. Zhou, J. C. Doyle, and K. Glover, *Robust and Optimal Control*. Prentice Hall, 1996.
- [27] B. K. Poolla, D. Groß, and F. Dörfler, "Placement and implementation of grid-forming and grid-following virtual inertia and fast frequency response," *IEEE Trans. Power Syst.*, vol. 34, no. 4, pp. 3035–3046, 2019.
- [28] A. Ademola-Idowu and B. Zhang, "Optimal Design of Virtual Inertia and Damping Coefficients for Virtual Synchronous Machines," in *IEEE Power and Energy Society General Meeting*, 2018.
- [29] L. Zhang, "Modeling and Control of VSC-HVDC Links Connected to Weak AC Systems," Ph.D. dissertation, KTH Royal Institute of Technology, 2010.



Enric Sánchez-Sánchez (S'15) received the Degree in Industrial Engineering from the School of Industrial Engineering of Barcelona, Technical University of Catalonia (UPC), Barcelona, Spain, in 2014, where he is currently pursuing a Ph.D. degree in Electrical Engineering. In 2012, he joined CITCEA-UPC as an Intern, where he became a Project Engineer in 2014. His research interests include modeling and control of power electronics converters integrated into the power system, HVDC transmission, and renewable generation systems.



Dominic Groß (S'11 - M'15) received a Diploma degree in Mechatronics from the University of Kassel, Germany, in 2010, and a Ph.D. degree (summa cum laude) in Electrical Engineering from the same university in 2014. From 2014 to 2015 he was with Volkswagen Group's Research Division in Wolfsburg, Germany. He is currently a Postdoctoral Researcher at the Automatic Control Laboratory at the Swiss Federal Institute of Technology (ETH) Zürich, Switzerland. His research interests include optimization based control, distributed control, and

analysis and control of complex networked systems with applications in power systems.



Eduardo Prieto-Araujo (S'12-M'16) received the degree in industrial engineering from the School of Industrial Engineering of Barcelona (ETSEIB), Technical University of Catalonia (UPC), Barcelona, Spain, in 2011 and the Ph.D. degree in electrical engineering from the UPC in 2016. He joined CITCEA-UPC research group in 2010 and currently he is a Serra Hünter Lecturer with the Electrical Engineering Department, UPC. His main interests are renewable generation systems, control of power converters for HVDC applications, interaction anal-

ysis between converters, and power electronics dominated power systems.



Florian Dörfler (S'09-M'13) is an Associate Professor at the Automatic Control Laboratory at ETH Zürich. He received his Ph.D. degree in Mechanical Engineering from the University of California at Santa Barbara in 2013, and a Diplom degree in Engineering Cybernetics from the University of Stuttgart in 2008. From 2013 to 2014 he was an Assistant Professor at the University of California Los Angeles. His primary research interests are centered around distributed control, complex networks, and cyber-physical systems currently with applications

in energy systems and smart grids. His students were winners or finalists for Best Student Paper awards at the 2013 European Control Conference, the 2016 American Control Conference, and the 2017 PES PowerTech Conference. His articles received the 2010 ACC Student Best Paper Award, the 2011 O. Hugo Schuck Best Paper Award, the 2012-2014 Automatica Best Paper Award, and the 2016 IEEE Circuits and Systems Guillemín-Cauer Best Paper Award. He is a recipient of the 2009 Regents Special International Fellowship, the 2011 Peter J. Frenkel Foundation Fellowship, and the 2015 UCSB ME Best PhD award.



Oriol Gomis-Bellmunt (S'05-M'07-SM'12) received the degree in industrial engineering from the School of Industrial Engineering of Barcelona (ETSEIB), Technical University of Catalonia (UPC), Barcelona, Spain, in 2001 and the Ph.D. degree in electrical engineering from the UPC in 2007. In 1999, he joined Engitrol S.L. where he worked as Project Engineer in the automation and control industry. Since 2004, he has been with the Electrical Engineering Department, UPC where he is a Professor and participates in the CITCEA-UPC Research

Group. His research interests include the fields linked with electrical machines, power electronics, and renewable energy integration in power systems.